Annu. Rev. Biomed. Eng. 2003. 5:251–84
doi: 10.1146/annurev.bioeng.5.011303.120714

First published online as a Review in Advance on April 18, 2003

MULTIAXIAL MECHANICAL BEHAVIOR OF BIOLOGICAL MATERIALS

Michael S. Sacks and Wei Sun

Engineered Tissue Mechanics Laboratory, McGowan Institute for Regenerative Medicine and the Department of Bioengineering, University of Pittsburgh, Pittsburgh, Pennsylvania 15219; email: msacks@pitt.edu

Key Words biaxial mechanical testing, constitutive modeling of planar biomaterials, homogeneity, mechanical properties of collagenous tissues

■ **Abstract** For native and engineered biological tissues, there exist many physiological, surgical, and medical device applications where multiaxial material characterization and modeling is required. Because biological tissues and many biocompatible elastomers are incompressible, planar biaxial testing allows for a two-dimensional (2-D) stress-state that can be used to fully characterize their three-dimensional (3-D) mechanical properties. Biological tissues exhibit complex mechanical behaviors not easily accounted for in classic elastomeric constitutive models. Accounting for these behaviors by careful experimental evaluation and formulation of constitutive models continues to be a challenging area in biomechanical modeling and simulation. The focus of this review is to describe the application of multiaxial testing techniques to soft tissues and their relation to modern biomechanical constitutive theories.

CONTENTS

1. INTRODUCTION

There exist many physiological, surgical, and medical device applications where rigorous soft tissue constitutive models are required. For biological materials, particular challenges in constitutive (stress-strain) modeling are encountered due to their complex mechanical behavior. For example, because of their oriented fibrous structures, they often exhibit pronounced mechanical anisotropy, nonlinear stress-strain relationships, large deformations, viscoelasticity, poroelasticity, and strong mechanical coupling. Taken as a whole, soft biological tissues defy simple material models.

Early biomechanical investigations of biological tissues were confined to uniaxial studies because of the difficulties in controlling two- (2-D) or even three-dimensional (3-D) boundary conditions. Due to the presence of mechanical anisotropy, uniaxial data cannot be used for parameter estimation in generalized 3-D constitutive equations, even if multidimensional strain data from the uniaxial experiment are available. There have also been investigations using inflation of circular membranes, which, under the assumption of isotropy, can provide the necessary experimental data (1, 2). Virtually all tissues are mechanically anisotropic; hence, this method cannot be generally applied. Further, when attempting to determine material constants for complex nonlinear constitutive models, testing methods are required that include comprehensive testing protocols that allow large variations in stress and strain states for accurate material parameter estimation (3).

For incompressible or nearly incompressible materials, biaxial mechanical testing can be used to obtain the material parameters for 3-D constitutive models. Biaxial testing of techniques was originally developed for studies of rubber elasticity (4, 5). In 1948, Treloar (4) pioneered techniques to apply two independently variable strains in two perpendicular directions with simultaneous measurement of the stresses. In 1951, Rivlin (5) developed a modified biaxial device that allowed for applied biaxial loads to rubber sheets, which allowed more precise experimental control. Using this device, Rivlin developed an integrated theoretical-experimental methodology in which the constitutive form could be derived and evaluated directly from multiaxial experimental data. This approach, and those that followed, greatly clarified the complex mechanical behavior of rubber, which can be confounded by such factors as material instabilities, physical aging, and Mullin's effect.

Biaxial experiments on soft biological tissues are generally difficult to perform and present challenges unique to biological tissues. Just a few of the experimental problems include small specimen sizes, structural and compositional heterogeneity, difficulty in gripping (without doing damage), dramatic effects of different gripping techniques (St. Venant–like effects), difficulty in precisely identifying material axes, difficulty in assuring constant forces along specimen edges, large specimen-to-specimen variability, and time-dependent changes due to biological degradation. In addition, a question of homogeneity of deformation within the specimen is paramount. These issues can often frustrate the application of even the most straightforward attempts to develop a constitutive model.

Biaxial testing devices have to be much more elaborate than uniaxial ones because of the need to control two boundary conditions. In particular, the edges must be able to expand freely in the lateral direction, and in the central target region the stress and strain states should be uniform so that data analysis can be performed simply. The target region must be small and located away from the outer edges to avoid the effects of specimen grips or tethers. Strain is measured optically to avoid any mechanical interference.

In addition to the above experimental issues, relating the observed mechanical response to tissue structure is perhaps more paramount than in other traditional material applications where the continuum scale is usually, at most, the size of large polymer molecules. In contrast, biological soft tissues are comprised of a dense network of collagen and elastin fibers, which indicates a continuum scale of typically ~ 1 μm. In addition, the fibers can undergo large rotations and exhibit nonlinear stress-strain behavior that can induce complex behaviors at the macro scale not easily accounted for in classic material models. Accounting for these behaviors in both experimental evaluation and formulation of appropriate constitutive models continues to be challenging.

The focus of this review is the application of multiaxial (primarily biaxial) testing techniques to soft tissues and their relation to relevant biomechanical constitutive theories. Although not an exhaustive review, major works of all investigators utilizing biaxial testing techniques for biological tissues known to the authors have been included. Finally, because biaxial testing and constitutive modeling has been the focus of much of the authors' recent work, the majority of the review focuses on the results of their studies.

1.1. A Note on the Notation System and Mechanics Theory

In general, the direct tensor notation adopted by Spencer (6) is followed. Here, tensors and vectors are represented using bold characters (e.g., **F**), whereas scalars are presented as normal text. Indicial notation is avoided for clarity of presentation. All mathematical operations are expressed in their equivalent matrix forms so that readers unfamiliar with tensor mathematics but who have a basic mathematical knowledge can follow the text. For those readers interested in a more comprehensive theoretical explanation of finite stress and strain tensors as well as relevant constitutive theories, please refer to (7–9).

2. BIAXIAL TESTING: KINEMATICS AND STRESSES

2.1. Basic Techniques for Biaxial Testing of Soft Biological Materials

In general, biaxial testing of biological tissues is performed using thin specimens, which are either a membrane in its native form or a thin section prepared from a thick tissue slab. The specimen is mounted to the biaxial device in trampoline-like fashion using thin threads, which allows the edges to expand freely in the lateral

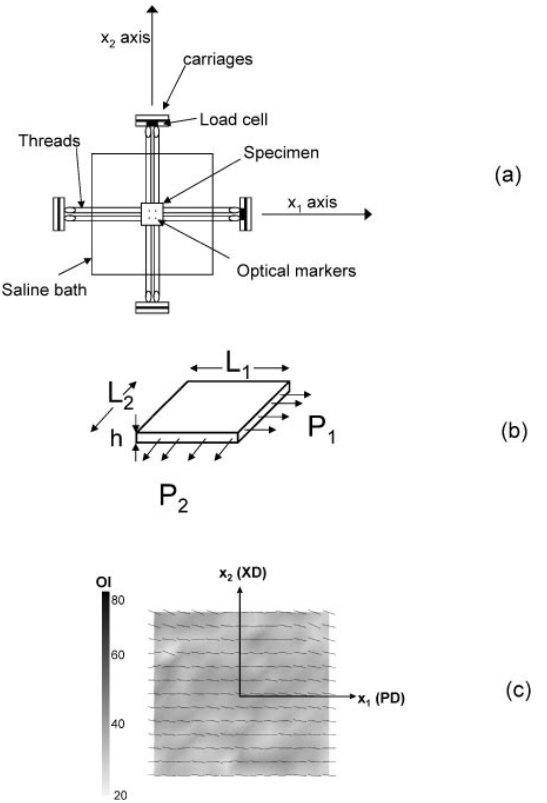

Figure 1 (*a*) Schematic of a biaxial testing device; (*b*) schematic of a biaxial specimen; and (*c*) a biaxial test specimen overlaid on a gray-scale representation of the degree of collagen fiber alignment using an orientation index (OI), demonstrating high uniformity of both fiber preferred directions and OI, along with the definition of the PD and XD axes.

direction (Figure 1*a*). Testing is generally performed with the specimen completely immersed in phosphate-buffered normal saline (pH 7.4) at room temperature or body (37°C) temperature. The central target region must be sufficiently small and located away from the outer edges to avoid the tethering effects (Figure 1*a*). Thus, in the central target region the stress and strain field is generally considered homogeneous.

2.2. Kinematics of a Biaxial Test

The following is a brief summary of the most important aspects of the kinematics of a biaxial mechanical test. For further details, the interested reader is referred to (7). We first consider the following homogeneous (i.e., independent of position) biaxial deformation:

$$x_1 = \lambda_1 X_1 + \kappa_1 X_2, \quad x_2 = \lambda_2 X_2 + \kappa_2 X_1, \quad x_3 = \lambda_3 X_3, \tag{1}$$

where x and X are position vectors representing the locations of material particles in the reference and deformed states, respectively, and λ_i are the axial stretch ratios and κ_i measures of in-plane shear. λ_i and κ_i are also components of the deformation gradient tensor **F**, which for deformation, as described in Equation 1, is

$$\mathbf{F} = \begin{bmatrix} \frac{\partial x_1}{\partial X_1} & \frac{\partial x_1}{\partial X_2} & \frac{\partial x_1}{\partial X_3} \\ \frac{\partial x_2}{\partial X_1} & \frac{\partial x_2}{\partial X_2} & \frac{\partial x_2}{\partial X_3} \\ \frac{\partial x_3}{\partial X_1} & \frac{\partial x_3}{\partial X_2} & \frac{\partial x_3}{\partial X_3} \end{bmatrix} = \begin{bmatrix} \lambda_1 & \kappa_1 & 0 \\ \kappa_1 & \lambda_1 & 0 \\ 0 & 0 & \lambda_3 \end{bmatrix}. \tag{2}$$

F is a critical mathematical quantity because it completely describes the deformation state. Because soft tissues are comprised primarily of water and have negligible permeability (8), they can be considered incompressible, so that $J = \det\mathbf{F} = 1$. From **F**, the right Cauchy-Green deformation tensor is defined as $\mathbf{C} = \mathbf{F}^T \cdot \mathbf{F}$, from which the components of the in-plane Green-Lagrange strain tensor $\mathbf{E} = {}^1\!/_2(\mathbf{C} - \mathbf{I})$, where **I** is the identity tensor. **E** is the most common finite strain measure in the soft tissue literature due to the simplicity of the constitutive formulations. In practice, the components of **E** are computed more directly using the following:

$$E_{11} = \frac{1}{2}\left(\lambda_1^2 + \kappa_2^2 - 1\right), \quad E_{12} = \frac{1}{2}\left(\lambda_1\kappa_1 + \lambda_2\kappa_2\right),$$
$$E_{22} = \frac{1}{2}\left(\lambda_2^2 + \kappa_1^2 - 1\right). \tag{3}$$

As mentioned above, the components of **F** are determined optically to avoid any mechanical interference with the specimen. This is typically done by tracking the position of markers mounted on the upper specimen surface that delimit the central target region using optical tracking software (10, 11) (Figure 1*a*). In both our laboratory (10) and in others (12, 13), finite element shape functions are used to approximate the position vector field within the central target regions. This can include linear and quadratic variations in strain (14).

2.3. Forces and Stress

As mentioned above, biaxial testing of biological tissues are performed using thin specimens (no more than ~3 mm, usually <1 mm) and acted on by only in-plane loads. A state of plane stress is thus assumed so that the components $t_{i3}(i = 1, 2, 3)$ of the Cauchy stress **t** (force/deformed area) are 0. Practically, during actual experiments, one can measure the initial specimen dimensions so that the Lagrangian stresses **T** (force/unit original cross-sectional area) are used for convenience. The components of **T** are computed from the measured axial forces **P** using:

$$T_{11} = \frac{P_1}{h L_2}, \quad T_{22} = \frac{P_2}{h L_1}, \tag{4}$$

where h is the specimen thickness and L_i is the specimen length (Figure 1*b*). Because experimentally applied loads are normal to the edges, $T_{12} = T_{21} = 0$. The second Piola-Kirchhoff stress tensor **S** is the most commonly utilized stress tensor for soft tissue constitutive theories and is determined using $\mathbf{S} = \mathbf{T}\,\mathbf{F}^{-1}$. The Cauchy stress tensor **t** is determined using $\mathbf{t} = \mathbf{F}\,\mathbf{T}/\mathbf{J}$, which in component form are given by (with $T_{12} = T_{21} = 0$):

$$t_{11} = \lambda_1 T_{11}, \quad t_{22} = \lambda_2 T_{22}, \quad t_{12} = \kappa_1 T_{22}, \quad t_{21} = \kappa_2 T_{11}. \tag{5}$$

In the case where there is negligible shear strain (i.e., $E_{12} \sim 0$), the normal components of the first and second Piola-Kirchoff stress tensors are related by:

$$S_{11} = T_{11}/\lambda_1, \quad S_{22} = T_{22}/\lambda_2. \tag{6}$$

3. ISOTROPIC ELASTOMERS

Perhaps the best way to introduce characterization and modeling for the multiaxial behavior of soft tissues is to summarize the pioneering work on elastomers of Treloar (4) and Rivlin (5, 15, 16). In addition to describing methods for multiaxial testing and modeling, the integrated mathematical-experimental approach of Rivlin is an excellent example on how to conduct material modeling in general. For this class of materials, we assume they are hyperelastic, which is defined as the existence of a strain energy function $W = W(\mathbf{F})$. W completely describes the change in internal (mechanical) energy of the material due to the application of external forces.

Because elastomeric materials are assumed to be isotropic, W is assumed be a function of the following strain coordinate invariants I_1 and I_2, defined as:

$$\begin{aligned} I_1 &= \mathrm{tr}\mathbf{C} = \mathrm{tr}\mathbf{B} \\ I_2 &= \frac{1}{2}[(\mathrm{tr}\mathbf{C})^2 - \mathrm{tr}\mathbf{C}^2] = \frac{1}{2}[(\mathrm{tr}\mathbf{B})^2 - \mathrm{tr}\mathbf{B}^2], \\ \mathbf{C} &= \mathbf{F}^{\mathrm{T}}\mathbf{F}, \quad \mathbf{B} = \mathbf{F}\mathbf{F}^{\mathrm{T}}, \end{aligned} \tag{7}$$

where **C** and **B** are known as the right and left Cauchy-Green deformation tensors, respectively (6). In this formulation, W is thus still a function of **F**, but it is restricted to isotropic materials through the coordinate invariance of I_1 and I_2. When there is no shear, $\kappa_1 = \kappa_2 = 0$.

Rivlin et al. (5) developed the following generalized strain energy formulation:

$$W = \sum_{i=0}^{\infty} \sum_{j=0}^{\infty} C_{ij} (I_1 - 3)^i (I_2 - 3)^j, \; C_{00} = 0, \tag{8}$$

where C_{ij} are material constants to be determined by fitting the model to experimental data. In most practical applications, the upper limits for the sums in Equation 8 are $I = j = 3$. For the homogenous deformation described by Equation 1, the

general constitutive model for isotropic elastomeric materials with $W = W(I_1, I_2)$ is expressed as (16):

$$t_{(ii)} = 2\left(\lambda_i^2 \frac{\partial W}{\partial I_1} - \frac{1}{\lambda_i^2}\frac{\partial W}{\partial I_2}\right) + p, \quad i = 1, 2, 3, \tag{9}$$

where p is a Lagrange multiplier that physically represents an arbitrary hydrostatic pressure, and the (ii) subscript indicates no component summation.

In addition to handling incompressibility explicitly using the Lagrange multiplier approach, one can also take advantage of the boundary conditions of a biaxial test to re-express the normal Cauchy stress components. Specifically, with $t_{33} = 0$ (upper and lower surfaces are traction free) and employing $\lambda_1\lambda_2\lambda_3 = 1$ to impose incompressibility, the two remaining Cauchy components are

$$\begin{aligned} t_{11} &= 2\left(\lambda_1^2 - \frac{1}{\lambda_1^2\lambda_2^2}\right)\left(\lambda_1^2 \frac{\partial W}{\partial I_1} - \frac{1}{\lambda_2^2}\frac{\partial W}{\partial I_2}\right), \\ t_{22} &= 2\left(\lambda_2^2 - \frac{1}{\lambda_1^2\lambda_2^2}\right)\left(\lambda_2^2 \frac{\partial W}{\partial I_1} - \frac{1}{\lambda_1^2}\frac{\partial W}{\partial I_2}\right), \end{aligned} \tag{10}$$

where the partial derivatives $\partial W/\partial I_1$ and $\partial W/\partial I_2$ are the response functions. Rather than assume an a-priori form, Rivlin noted that response functions can be determined directly from the experimental measured variables using

$$\frac{\partial W}{\partial I_1} = \frac{\frac{\lambda_1^2 t_{11}}{\lambda_1^2 - \frac{1}{\lambda_1^2\lambda_2^2}} - \frac{\lambda_2^2 t_{22}}{\lambda_2^2 - \frac{1}{\lambda_1^2\lambda_2^2}}}{2\left(\lambda_1^2 - \lambda_2^2\right)} \qquad \frac{\partial W}{\partial I_2} = \frac{\frac{t_{11}}{\lambda_1^2 - \frac{1}{\lambda_1^2\lambda_2^2}} - \frac{t_{22}}{\lambda_2^2 - \frac{1}{\lambda_1^2\lambda_2^2}}}{2\left(\lambda_2^2 - \lambda_1^2\right)}. \tag{11}$$

Thus, by conducting constant invariant biaxial tests the functional form of W can be directly determined from the experimental data. This approach can avoid much of the ambiguity inherent in constitutive modeling of elastomeric materials. This problem should not be underestimated because other than the statement of the basic form $W = W(\mathbf{F})$, there are no other general theoretical restrictions to guide the form of W as in linear elasticity.

4. FIRST BIAXIAL MECHANICAL STUDIES OF BIOLOGICAL TISSUES

4.1. Fung and Coworkers

The first investigators to develop and utilize planar biaxial testing for soft biological tissues were Lanir & Fung in 1974 (17, 18), who investigated the mechanical properties of rabbit skin. Briefly, a 3-cm to 6-cm square skin specimen was mounted in a trampoline-like fashion with up to 68 individual attachments distributed equally over the four specimen sides (17/side). Similar to Rivlin (5), the tension on each line could be individually adjusted to insure a reasonably uniform stress was

applied to each specimen side. Actuator motion was controlled utilizing a function generator. To avoid the effects of local stress concentrations of the suture attachments, bidirectional tissue strain was measured in a central region by monitoring the distance between pairs of lines separated by ~5 mm along each axis video dimensional analyzers (VDAs) (19). Briefly, a VDA is an electronic device the works with a video camera signal to convert the distance between two dark-light or light-dark transitions in the image to a linearly proportional voltage, which can be recorded and converted to displacement. Typically, soft tissues are light in color so that the distance between dark lines applied to the tissue surface are tracked in real time. The advantage of the VDA is that it allows for noncontacting, real-time displacement measurements directly using conventional video. For biaxial studies, Lanir & Fung utilized two orthogonally positioned VDAs with a common optical path to allow for simultaneous, synchronized displacement measurements along each stretch axis.

Experimental results demonstrated that skin exhibited a nonlinear, orthotropic stress-strain response, whose material axis depended on the specimen's anatomic orientation. Although differences between the loading and unloading curves were observed due to hysteresis, the loading and unloading stress-strain responses were essentially independent of strain rate. It is important to note that these results underscore the major phenomenon found in all subsequent biaxial mechanical investigations of soft planar tissues.

Based on these experimental observations and data, Tong & Fung (20) used the above biaxial data to develop a constitutive model. Because of the insensitivity to strain rate, separate pseudo strain-energy functions could be developed for the loading and unloading phases of the stress-strain curve (8). Thus, for the loading and unloading phases. the in-plane second Piola-Kirchhoff stresses are derived from a 2-D strain energy function W:

$$S_{ij} = \frac{\partial W}{\partial E_{ij}}. \tag{12}$$

For the form of W, Tong & Fung observed from the experimental data that the stress-strain curves had a very shallow slope followed by an abrupt transition to a very high stiffness. Due to this biphasic-like behavior, they started with the generalized form:

$$\rho_0 W = \frac{1}{2}\left(\alpha_1 E_{11}^2 + \alpha_2 E_{22}^2 + \alpha_3\left(E_{12}^2 + E_{21}^2\right) + 2\alpha_4 E_{11}E_{22}\right) + \left[\frac{c}{2}\exp\begin{pmatrix} a_1 E_{11}^2 + a_2 E_{22}^2 + a_3\left(E_{12}^2 + E_{21}^2\right) + 2a_4 E_{11}E_{22} \\ + \gamma_1 E_{11}^3 + \gamma_2 E_{22}^3 + \gamma_4 E_{11}^2 E_2 + \gamma_5 E_{11}E_{22}^2 \end{pmatrix} - 1\right], \tag{13}$$

where ρ_0 is the initial tissue density; α_i, a_i, and γ_i are material constants, and E_{ij} is the Green strain tensor. This form is able to model both the low- (first term on the right-hand side) and high-stress (second term on the right-hand side) regions of the stress-strain curve.

In practice, Equation 13 contains many more terms than is actually necessary to model the stress-strain curve. For all practical purposes, the α_i and γ_i terms are not necessary to obtain a satisfactory fit to the majority of the stress-strain curve, especially the higher stress regions. Thus, Equation 13 can be reduced to the "Fung" type (which incidentally was found to fit the data almost as well):

$$\rho_0 W = \frac{c}{2}(e^Q - 1), \tag{14}$$

where $Q = c_{ijkl}E_{ij}E_{kl}$. In practice, in biaxial testing, the shear strain E_{12} is nearly zero, so that Equation 14 can be written as:

$$\rho_0 W = \frac{c}{2}\left[\exp\left(a_1E_{11}^2 + a_2E_{22}^2 + 2a_4E_{11}E_{22}\right) - 1\right]. \tag{15}$$

This is perhaps the most broadly used constitutive model to date for the biaxial response of soft biological tissues (as well as other loading states), including skin (20), pericardium (21), epicardium (22), visceral pleura (23), and myocardium (see below).

One of the difficulties in applying Equation 14 to biological tissue is the high amount of interspecimen variability, which, in turn, translated into wide variability in material parameter values. The sources of variability have been attributed to experimental noise, numerical instability of the fitting algorithms resulting from the nonlinearity of Equation 14, and strain history dependence of the tissue. These problems can confound the ability to obtain a unique set of material constants either for a given specimen or a class of biomaterials. Further, the residuals in nonlinear regression may not be normally distributed, disallowing conventional statistical analysis.

In their study of canine pericardium, Yin et al. (24) developed a statistical-based approach to assess the sources of and account for the variability in material constants in describing biaxial stress-strain data. Using experimental data for canine pericardium (21), they determined a strain energy function (including exploring the use of noninteger powers of the Green strain). They performed a residual analysis to determine if standard statistical methods could be used to assess the variability, and if not, then they used nonparameteric methods (bootstrapping). Using a five-parameter exponential strain energy function, pericardial tissue was found to be strain-history dependent and anisotropic, which could not be attributed to either experimental noise or instability in the numerical algorithms.

4.2. Vito and Coworkers

Another group active in the developing multiaxial constitutive relationships was Vito and coworkers. Among the technical improvements of their device were the use of multiparticle tracking to allow computation of the complete in-plane strain tensor and the use of real-time computer control (25). Perhaps their main contribution was the development of a technique to identify the specimen's material axis (3). Generally, identification a material axis is based on observations of the

gross specimen shape (e.g., long axis of a blood vessel) or gross fiber architecture (e.g., myocardium). However, in many tissues, the fibers are too small to be visually observed, and up to the time of the study there were no rapid, nondestructive techniques for quantification of fiber architecture.

In Choi & Vito's technique, they identified the material axis by determining which directions, when loaded to the same stress, demonstrated the greatest and least strain values. To demonstrate their approach, Choi & Vito (3) utilized canine pericardium, a thin membrane that surrounds the heart. The pericardium functions to restrict excessive dilation of the heart during filling; is involved with the hemodynamic interaction of the heart's right and left ventricles; and in humans, provides mechanical support to the diaphragm. It is comprised primarily of collagen, a fibrous protein (the most common in the body) that possesses high tensile strength, and is thus found in tissues that require significant mechanical strength or provide structural support. To determine the orientation of the material axes, round pericardial tissue specimens were prepared, with opposing pairs of small clamps placed throughout the specimen's perimeter in 15° increments. For each opposing pair, the specimen was preloaded, and two marks were made aligned to the stretch axes. This procedure was repeated for each successive attachment pair. When fully unloaded, the markers produced an ellipsoidal pattern whose semiaxes were aligned to the material axes.

To perform the biaxial tests, a square biaxial test specimen was cut from the original circular specimen, with edges aligned parallel and perpendicular to the material axis as determined above. Multiple test protocols were used to obtain stress-strain data under multiple loading states. Practically, this was accomplished using constant ratios of strain or stress during each protocol, with a sufficient number of protocols and ratios chosen to cover the complete E_{11}-E_{22} or S_{11}-S_{22} plane. Choi & Vito (3) then used the following strain energy function for the canine pericardium biaxial mechanical data:

$$\rho_0 W = b_0 \left[\exp\left(b_1 E_{11}^2\right) + \exp\left(b_2 E_{22}^2\right) + \exp\left(2b_3 E_{11} E_{22}\right) - 3\right], \quad (16)$$

where b_i are material constants. They demonstrated that when data from a single test protocol was used to determine the values for b_i, different values were obtained for each protocol. Only when the data from all protocols was used simultaneously were the "true" material constants obtained for the specimen. This was shown to be due to the presence of multiple collinearities due to the use of constant E_{11}:E_{22} or S_{11}:S_{22} ratios. This concept was extended to the multiaxial testing of blood vessels (26).

Although the values for the b_i were rigorously obtained and the model was shown to work well under strain control tests, it did not work as well under load control tests. The reason underlying this disagreement is at present unknown and suggests a need for experimental and theoretical investigations of constitutive theories that can better handle mixed boundary conditions. Another problematic finding with canine pericardium is the substantial variability in both degree of anisotropy (varying from quasi-isotropic to moderately anisotropic), which translated into significant interspecimen variability in material constants. Thus, although reliable

material parameters for Equation 16 may be reliably obtained for an individual specimen, generic material parameters for canine pericardium could not be obtained. This problem was addressed by Sacks (10) and is described in detail in Section 5.1.

4.4. Alternative Approaches to Determining Strain Energy Functions

Although based on rigorous experimental data and able to capture the 2-D in-plane biaxial response well, the constitutive models described above present certain difficulties both in terms of their form and parameter determination. In particular, although based on fundamental mechanics principals, there is no additional knowledge to guide the particular choice of form of the model and it is somewhat arbitrary. Models are generally evaluated for the degree of overparameterization using comprehensive statistical methods [e.g., (24)] and subsequently modified, generally in the reduction of the number of parameters.

Following methods analogous to those developed by Rivlin et al. for rubber elasticity (5), Humphrey et al. developed a new functional form for myocardium biaxial mechanical properties. In this approach, Humphrey defined a subclass of transversely isotropic materials that are a function of two strain invariants (27):

$$W = W(I_1, I_4), \tag{17}$$

where I_1 and I_4 are the first and fourth strain invariants, with $I_4 = \alpha^2$ where α is the stretch ratio along the muscle fiber direction. Similar to the approach by Rivlin, this form allows determination of the dependence of W_1 and W_α on I_1 and α directly from the experimentally obtained stress and deformation data (27):

$$2W_1 = \frac{\xi_4 t_{11} - \xi_2 t_{22}}{\xi_1\xi_4 - \xi_2\xi_3} \qquad W_\alpha = \alpha\frac{\xi_1 t_{22} - \xi_3 t_{11}}{\xi_1\xi_4 - \xi_2\xi_3}, \tag{18}$$

where $W_1 = \partial W/\partial I_1$; $W_\alpha = \partial W/\partial\alpha$; t_{ij} are the physical components of the Cauchy stress tensor; and

$$\begin{aligned}
\xi_1 &= \lambda_1^2 + \kappa_1^2 - \lambda_3^2 \\
\xi_2 &= \lambda_1^2 \cos^2(\theta) + 2\lambda_1\kappa_1 \cos(\theta)\sin(\theta) + \kappa_1^2 \sin^2(\theta) \\
\xi_3 &= \lambda_2^2 + \kappa_2^2 - \lambda_3^2 \\
\xi_4 &= \kappa_2^2 \cos^2(\theta) + 2\lambda_2\kappa_2 \cos(\theta)\sin(\theta) + \lambda_2^2 \sin^2(\theta) \\
\xi_5 &= \kappa_1\lambda_2 + \kappa_2\lambda_1 \\
\xi_6 &= \lambda_1\kappa_2 \cos^2(\theta) + (\lambda_1\lambda_2 + \kappa_1\kappa_2)\cos(\theta)\sin(\theta) + \kappa_1\lambda_2 \sin^2(\theta),
\end{aligned} \tag{19}$$

where λ_i and κ_i are components of the deformation gradient tensor and θ is the fiber angle with respect to the x_1 axis. Next, based on experimental plots of W_1

and W_α versus I_1 and α, they assumed the following functional form for $W(I_1, \alpha)$:

$$W(I_1, \alpha) = \sum_{i=0}^{n} \sum_{j=0}^{m} c_{ij} (I_1 - 3)^i (\alpha - 1)^j, \quad (20)$$

where c_{ij} are material parameters. The interested reader is referred to (27) for details of the derivation.

To apply this approach, Humphrey et al. (27) modified their biaxial testing device to perform constant strain invariant tests. From the experimental data generated, plots of W_1 and W_α versus either I_1 varied and α held constant or I_1 held constant and α varied were generated using Equations 18 and 19. Based on the resulting response functions as well as theoretical restrictions on the values of c_{ij} [e.g., at zero strain $W(3, 1) = 0$, requiring $c_{00} = 0$], the following form for passive myocardium was derived:

$$W(I_1, \alpha) = c_1(\alpha - 1) + c_2\alpha - 1)^3 + c_3(I_1 - 3) + c_4(I_1 - 3)(\alpha - 1) + c_5(I_1 - 3)^2, \quad (21)$$

where c_i are the material constants. In obtaining the material constants, additional empirical inequalities were applied to set bounds on the values for c_i.

The constant invariant tests used to derive Equation 21 require that the tissue specimen be subjected to simultaneous loading and unloading, which strictly violates pseudoelasticity (8). Thus, only data from the loading portion of the equibiaxial strain and constant α tests were used to determine values for c_i. The data from constant I_1 tests were used only to find the functional form, and were hence excluded because the tissue experiences simultaneous loading and unloading during these tests. The resulting model was found to fit the biaxial data quite well, and was also found not to be overparameterized (28). The results also emphasized the need for good data, including accurate measurement of the applied forces, original dimensions, and experimental deformations. Sacks & Chuong (29) later successfully applied Equation 21 to right ventricular myocardium, where the effects of a fiber splay within the specimen were incorporated. May-Newman also applied a similar approach to the biaxial mechanical properties of the mitral valve (30). It is also interesting to note that the overall approach of using theoretically guided experiments is not restricted to the form of Equation 20, but also has been successfully applied to the epicardium (a thin connective tissue layer surrounding the heart) (22) using the Fung model (Equation 14) and constant E_{11} and E_{22} tests.

Clearly, the strength of the above approach is that it allows derivation of functional form of W to be rigorously based on direct evaluation of the experimental data. This avoids the limitations of the trial-and-error approach of earlier work and is an elegant example of how theory and experiment can be successfully integrated. In principal, the approach can be applied to specimens where there is a nonzero distribution of fiber orientations. However, the lead author has found the model to be weakly dependent with respect to transmural layer orientations, potentially due to transverse isotropy assumption (M.S. Sacks, unpublished data).

More detailed, realistic interlayer models may need to be developed. Further, in order to determine the form of W, strict pseudo-elasticity must be violated (i.e., the tissue must be subjected to simultaneous loading and unloading protocols). Although the loading and unloading curves are qualitatively similar, differences do exist and may influence the sensitivity and final choice of the form.

5. RECENT DEVELOPMENTS

5.1. Control of Specimen Structure

A reoccurring difficulty in many of the above studies, particularly for collagenous tissues such as skin and pericardium, is the substantial degree of interspecimen variability. This variability underscores the need to determine the source of the underlying biological variability for accurate and meaningful determination of material constants. This is a particular problem when using biologically derived tissues in medical devices (e.g., bioprosthetic heart valves), where accurate constitutive models are essential for device design, determining effects of novel chemical treatments, and understanding the simulation of fatigue damage. One such tissue is chemically treated bovine pericardium: Although mechanically anisotropic (31, 32), there is no evidence that bioprosthetic heart valves are constructed to accommodate or take advantage of this anisotropy in a systematic way. Finite element stress analyses of bioprosthetic heart valves suggest that high flexural stresses during valve opening and high tensile stresses during valve closure are associated with failure locations (33–35). Their accuracy, however, is limited by the use of simplistic isotropic material approximations because, in reality, chemically treated bovine pericardium is an anisotropic, biocomposite material.

To quantify the fibrous structure of planar tissues, Sacks et al. (36) have developed a small-angle light scattering technique (SALS). SALS allows for rapid quantification of the angular distribution of fibers at each point in the tissue, from which the preferred fiber direction and degree of orientation can be determined. A SALS-based tissue-sorting procedure was used to guide the selection of bovine pericardial specimens to minimize structural variability (10). Note that in this study, the designations preferred fiber (PD) and cross-preferred fiber (XD) were used for the x_1 and x_2 axes, respectively (Figure 1*b*). An extensive biaxial test protocol was then used and the resulting stress-strain data was fitted to an exponential strain energy function developed by Choi & Vito (3). Results indicated that this equation was able to reproduce the mechanical response of chemically treated bovine pericardium over a wide range of biaxial test protocols. Most importantly, the high structural uniformity resulted in both a consistent mechanical response and low variability in the material constants.

Because of this consistency, the data from all specimens were combined into a single dataset. From this dataset, "group" material constants were determined, which represent a more generalized estimate of tissue properties. The individual specimen constants showed predictably better agreement with the data, but the

group constants were able to represent the data reasonably well. This study demonstrated that much of the past difficulties with tissue variability were a direct result of uncontrolled variability in tissue structure. Previous studies on myocardium (28, 29, 37) controlled specimen structure by visual selection and alignment to the overall preferred fiber direction. This was an important step in the analysis of orthotropic biological tissues. The use of SALS, however, not only allowed similar specimen fiber alignment for collagenous tissues, but more importantly, showed the quantitative relation between the degree of fiber alignment and degree of mechanical anisotropy. To the authors' knowledge, this is the first time such a comparison was undertaken for fibrous collagenous tissues.

In addition to minimizing tissue variability, tight control of tissue structure allows elucidation of the more subtle aspects of tissue mechanical properties. In our previous studies on pericardial mechanical properties, we observed that the strain level along the x_1 axis (or PD direction, Figure 1*a*) has a stronger effect on the x_2 axis stress level (or XD, Figure 1*a*) than the x_2 axis strain level has on the x_1 axis stress level (38). While this phenomenon has been termed coupling, it is distinct from the expression $\frac{\partial}{\partial E_{11}}\left(\frac{\partial W}{\partial E_{22}}\right) = \frac{\partial}{\partial E_{22}}\left(\frac{\partial W}{\partial E_{11}}\right)$, which holds at a particular strain state (E_{11}, E_{22}). In contrast, the phenomenon referred to here deals with how stress magnitudes along one axis are affected by the strain level along the perpendicular axis. Similar mechanical coupling properties have been reported for mitral valve leaflets (39) and for passive myocardium [e.g., figure 4 in (40)]. Work by the Sacks group using a structural constitutive approach has demonstrated that this effect is a direct result of the particular architecture of the pericardium's collagen fibers. This architecture can produce complex mechanical behaviors at the tissue level due to large fiber strains and rotations, along with a nonlinear fiber stress-strain relationship (41, 42).

5.2. Effects of In-Plane Shear

A limitation in virtually all planar biaxial studies of soft tissues has been the inability to include the effects of in-plane shear. This is due to the inability of current mechanical testing devices to induce a state of in-plane shear due to the added cost and complexity. We have developed a straightforward method for planar biaxial testing that induces a combined state of in-plane shear and normal strains (43). The method relies on rotation of the test specimen's material axes, with respect to the device axes, and on rotating carriages to allow the specimen to freely undergo in-plane shear.

To demonstrate this method, five glutaraldehyde-treated bovine pericardium (GLBP) specimens were prepared with their preferred fiber directions (defining the material axes) oriented at 45° to the device axes to induce a maximum shear state (Figure 2*a*). The test protocol included a wide range of biaxial strain states, and the resulting biaxial data re-expressed in the material axes coordinate system. The resulting biaxial data was then fit to the following strain energy function W:

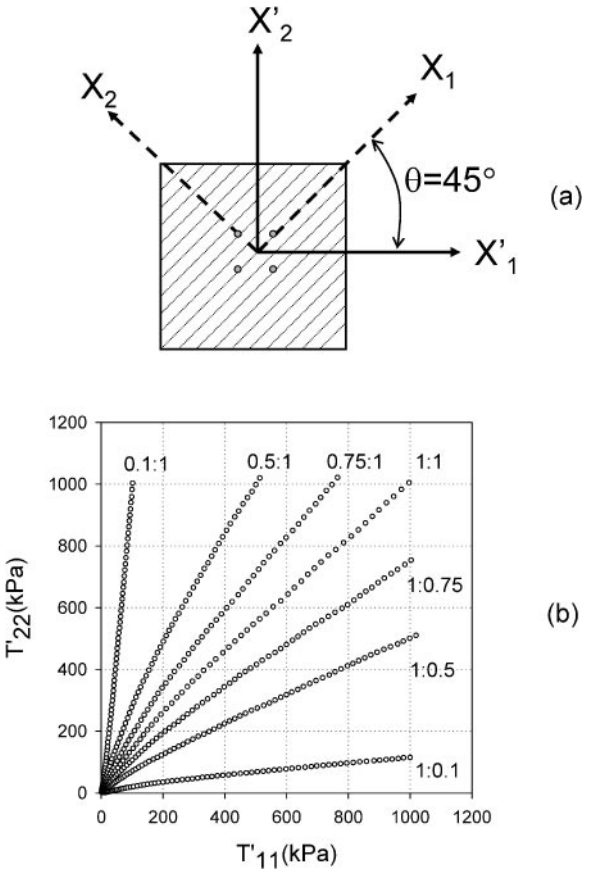

Figure 2 (*a*) A schematic of the biaxial specimen showing the specimen axes ($X'_1 - X'_2$ axes) and material axes (i.e., $X'_1 - X'_2$ axes), which was aligned at a 45° angle with respect to the specimen axes. (*b*) Experimental protocols of stress-control biaxial testing, where the labels indicate the ratios of the normal Lagrangian stress in the specimen axes coordinate system ($T'_{11} : T'_{22}$).

$$W = \frac{c}{2}\Big[\exp\left(A_1E_{11}^2 + A_2E_{22}^2 + 2A_3E_{11}E_{22} + A_4E_{12}^2 + 2A_5E_{11}E_{12} + 2A_6E_{22}E_{12}\right) - 1\Big], \quad (22)$$

where E_{ij} are the components of the Green strain tensor expressed in the material axes coordinate system and c and A_i are constants. Whereas W was able to fit the data very well, the constants A_5 and A_6 were found not to contribute significantly to the fit and were considered unnecessary to model the shear strain response. Although not able to independently control the amount of shear strain or induce a state of pure shear, the method presented readily produces a state of simultaneous

in-plane shear and normal strains. The method is very general and can be applied to any anisotropic planar tissue that has identifiable material axes. However, peak nominal stresses in the study cited above were limited to ∼250 kPa and peak shear stresses to ± 40 kPa. Other applications, such as novel heart valve biomaterials, may be subjected to larger in-plane shear strains. Clearly, robust constitutive models require a comprehensive experimental dataset that spans the estimated normal operational stress range.

Sun et al. (44) recently conducted a study to produce biaxial mechanical experimental strain over a wide range of normal and shear stresses by modifying our strain-based biaxial testing protocol to a stress-based one using peak stresses of 1 MPa. As in our previous study, GLBP was utilized as the representative soft tissue biomaterial. The stress-controlled biaxial protocol covered a wide range of strain-stress space (Figure 2*b*). Of particular note are the high in-plane shear stresses generated (peak ∼400 kPa) at a peak shear strain of ± 0.10 (Figure 3*b*), which are comparable in magnitude to the corresponding normal stress and extensional strain components (Figure 3*a*,*c*). A feature of the GLBP biaxial response we have not previously observed was that the responses to the $T'_{11} : T'_{22} = 1 : 0.1$ and 0.1 : 1 "outer" protocols were different from the "inner" five protocols ($T'_{11} : T'_{22} = 1 : 0.5$, 1:0.75, 1:1, 0.75:1, 0.5:1; Figure 2*b*). The outer two protocols exhibited not only large shear response, but also lesser extensibility for the normal components. This behavior suggested a substantial change in mechanical behavior under the extreme $T'_{11} : T'_{22}$ ratios, where the shear stresses were greater by approximately twofold or more compared to the other test protocols.

Given the substantially more complex tissue response using the stress-controlled protocol, it was not surprising that Equation 22, albeit containing two additional degrees of freedom from our earlier model (43), was still not sufficiently improved. In particular, Equation 22 had difficulties with the shear response of the 1:0.1 and 0.1:1 protocols. Based on our current observations (Figure 3), we hypothesized that the high shear state occurring in the outer two protocols was a primary factor in our poor fit results. We therefore subdivided the experimental data into two sets: Set I was composed of the "inner" five protocols ($T'_{11} : T'_{22} =$ 1:0.5, 1:0.75, 1:1, 0.75:1, 0.5:1 protocols) and Set II was composed of the "outer" two protocols ($T'_{11} : T'_{22} =$ 0.1:1 and 1:0.1). Next, we applied this approach using Equation 3, which was able to describe each individual dataset well (Figure 4), with Set I $r^2 =$ 0.980 and Set II $r^2 =$ 0.963. These results suggest that a Fung-type model using Equation 22 was adequate using two separate sets of material constants for the low/moderate and high shear states.

Although able to fit the biaxial data, a single analytical expression was clearly preferable. This was underscored by the limited predictive abilities of the subdivided model. For example, we expected that Equation 22 could predict the Set I response using the Set II parameters reasonably well because the Set I strain range lies within the Set II strain space. However, the results for this interpolation were poor (Figure 5). Given the complexity of the strain space, improper subdivision could lead to highly erroneous stress predictions.

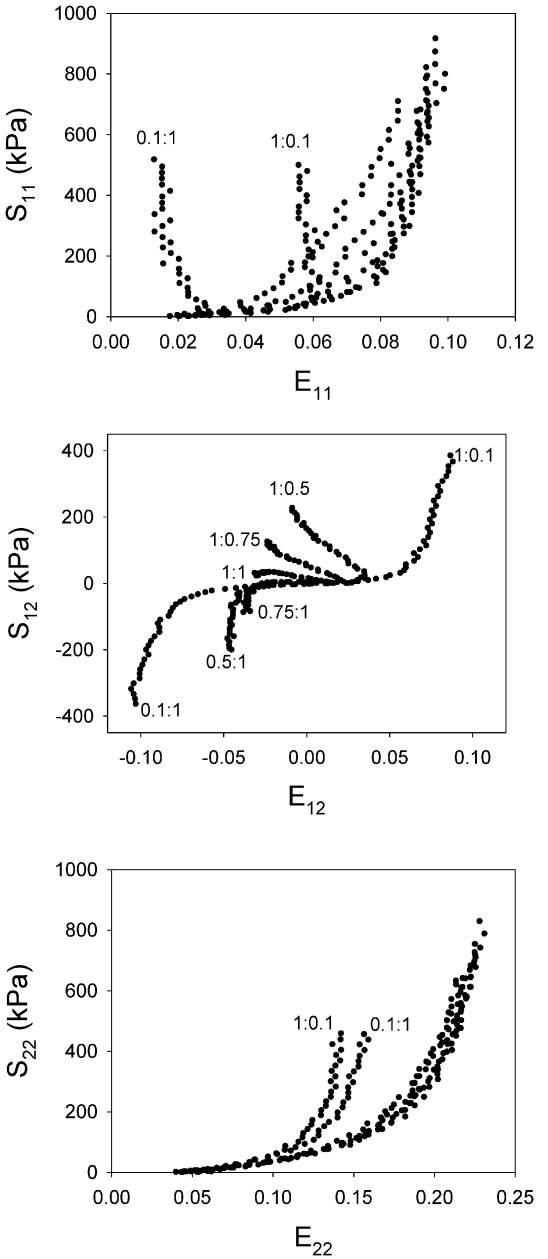

Figure 3 A representative biaxial mechanical response for each component, with peak shear stresses of 400 kPa and peak shear strains of ± 0.10. One novel feature observed was that the mechanical response to the $T'_{11} : T'_{22} =$ 1:0 and 0:1 were quite different from the other protocols. Labels indicate the ratios of the normal Lagrangian stress in the specimen axes coordinate system ($T'_{11} : T'_{22}$).

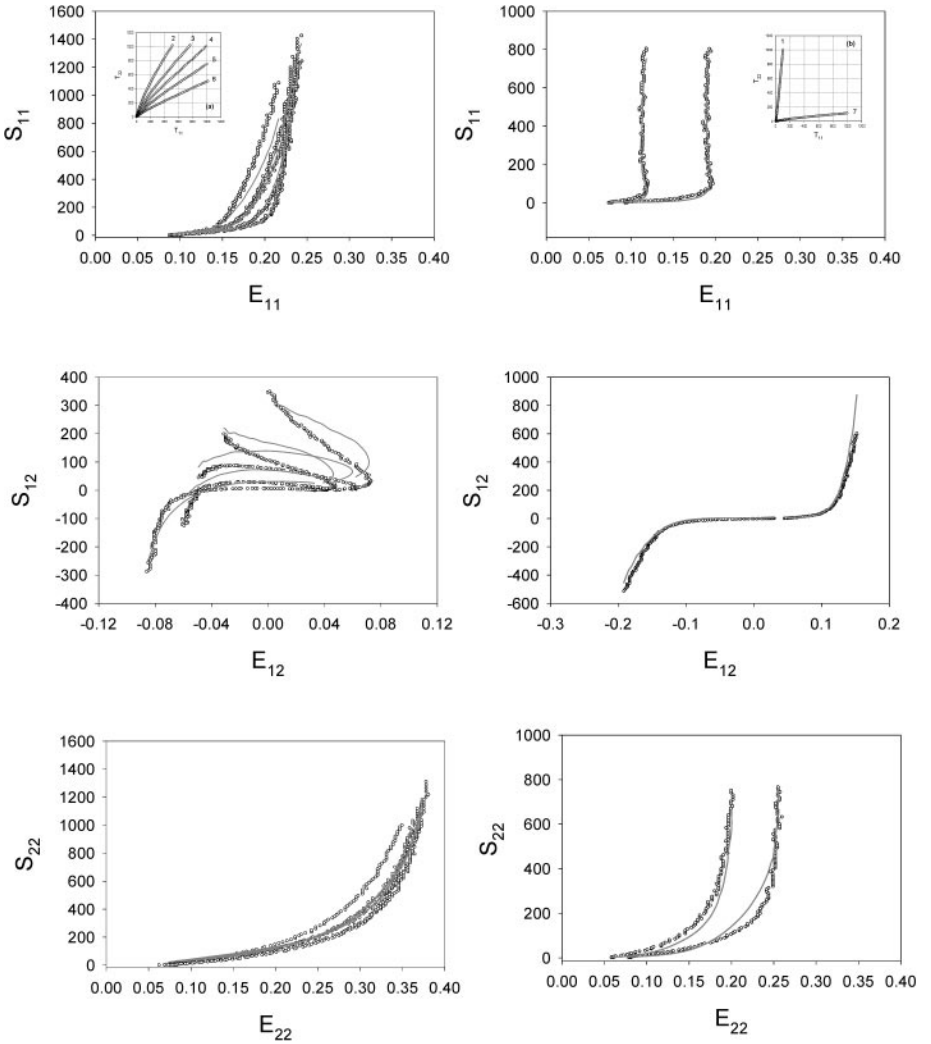

Figure 4 Results for the seven-parameter Fung model applied to (*a*) the subdivided dataset I, demonstrating a very good fit ($r^2 = 0.980$), and dataset II, demonstrating a very good fit ($r^2 = 0.963$). Inset: biaxial protocols for each protocol set.

To develop a single model for all protocols, we expanded Equation 22 as follows: To minimize the number of parameters, we chose to modify Q only through the addition of quartic order terms. Although cubic order terms of the general form could have been added, it was felt that quartic functions of the form would be more numerically robust and able to simulate complex mechanical responses with fewer parameters. Thus, the final generalized form for the expanded Q (incorporating

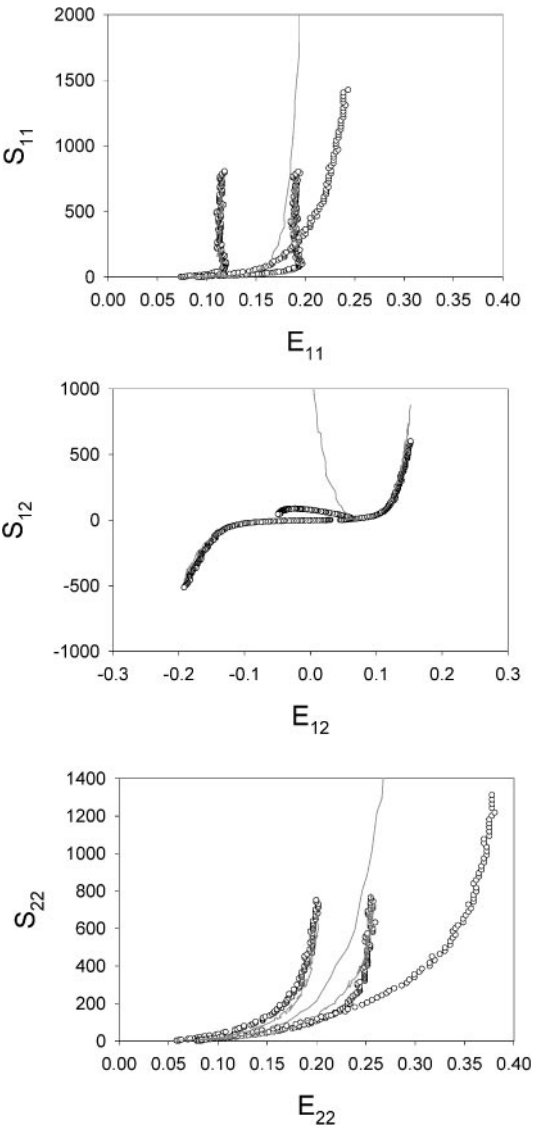

Figure 5 Predictive capability results for the equal-biaxial protocol 1:1 by fitting the seven-parameter model to the $T'_{11} : T'_{22} = 1{:}0.1$ and $0.1{:}1$ protocols only. Even though equal-biaxial protocol lies within the stress and strain ranges used for parameter determination, the interpolated result is poor. For illustration purposes, the peak values of S_{11}, S_{12}, and S_{22}, which were 1.4e+5, 0.4E+5, and 1.2E+5 kPa, respectively, were truncated.

symmetry of **E**) is given by:

$$Q = A_1E_{11}^2 + A_2E_{22}^2 + 2A_3E_{11}E_{22} + A_4E_{12}^2 + 2A_5E_{12}E_{11} + 2A_6E_{12}E_{22} + B_1E_{11}^4 + B_2E_{22}^4 + B_3E_{11}^2E_{22}^2 + B_4E_{12}^4 + B_5E_{12}^2E_{11}^2 + B_6E_{12}^2E_{22}^2, \quad (23)$$

where A_i and B_i are the material constants.

As in any nonlinear constitutive model, the number of term additions needs to be minimized to avoid numerical instability issues in computational implementations. To provide a rationale for adding the additional quadric terms in Equation 23, we developed the following interpolation method to estimate the strain energy response functions with respect to each strain component directly from our stress-controlled biaxial test data. Each **S** component from the loading data was expressed as a function of two strain components, whereas the third component was kept at a constant value. This allowed us to simulate the pseudo-elastic loading response of each **S** component against various combinations of **E** and guide the choice of the functional form of **Q**. Interpolations were restricted over the strain space of the actual experimental data. Details of the approach are presented in (44). All together, nine response functions were generated, three for each stress component.

Representative response functions are shown in Figure 6*a* for S_{12}, where E_{11} and E_{12} were varied and E_{22} was held at 0.2. In this case, the response function indicated that S_{12} had a relatively weak dependence on E_{11}. This indicated that additional terms did not require E_{11}, so that B_1, B_3, and $B_5 = 0$. Figure 6*b* also shows S_{12} where E_{11} and E_{22} were varied and E_{11} was held at 0.18. The response function indicated that S_{12} had a strong dependence on E_{12} and E_{22}. Based on the more gradual increase in stress of the stress-strain curves, we determined that inclusion of quartic powers for individual strain components (i.e., E_{ij}^4) was unnecessary, thus $B_2 = B_4 = 0$, leaving only the term $B_6E_{12}^2E_{22}^2$. Replacing B_6 with B, we derived the following eight-parameter form for the expanded Fung-type model:

$$Q = A_1E_{11}^2 + A_2E_{22}^2 + 2A_3E_{11}E_{22} + A_4E_{12}^2 + 2A_5E_{12}E_{11} + 2A_6E_{12}E_{22} + BE_{12}^2E_{22}^2. \quad (24)$$

Equation 24 was found to describe the biaxial mechanical response for all seven protocols well, with a mean $r^2 = 0.94$. Bootstrapping results indicated that the parameters were highly clustered for the simulated datasets, giving further confidence in the uniqueness of the model parameter values and model robustness. The predictive capability of Equation 24 was evaluated by fitting the Set I data only and then extrapolating Set II (Figure 7*a*). As expected, Equation 24 demonstrated a better fit to Set I alone (Figure 7*a*) than when Sets I and II were fit simultaneously (Figure 7*b*), especially the in-plane shear response. Interestingly, this approach also demonstrated good predictive capabilities (Figure 7*a*). Overall, Equation 24 was able to faithfully reproduce the complete high in-plane response and predict the tissue response outside the range used for parameter determination.

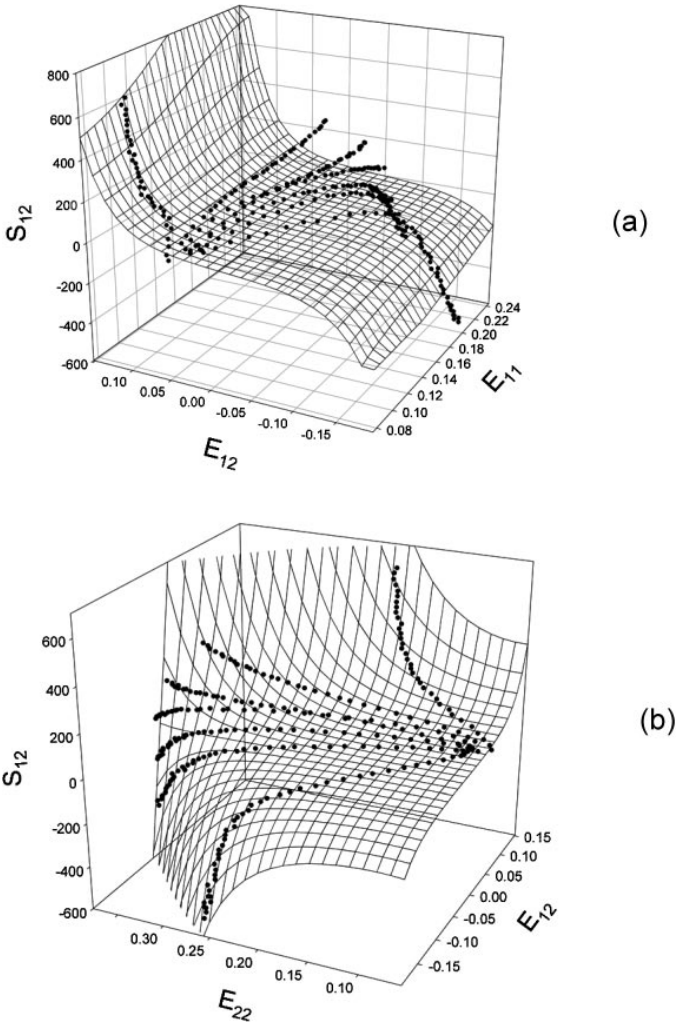

Figure 6 Representative response functions for (*a*) S_{12} versus E_{11} and E_{12}, with $E_{22} = 0.2$, indicating that S_{12} had a relatively weak dependence on E_{11}. In contrast, the S_{12} versus E_{12} and E_{22}, with $E_{11} = 0.18$, responses shown in (*b*) indicated that S_{12} had a strong dependence on both E_{12} and E_{22}.

6. STRUCTURAL CONSTITUTIVE MODELS

Although the phenomenological constitutive models discussed above were successful in the above applications, they are unable to elucidate the underlying mechanisms of tissue behavior. Structural constitutive models attempt to integrate information on tissue composition and structure to avoid ambiguities in material

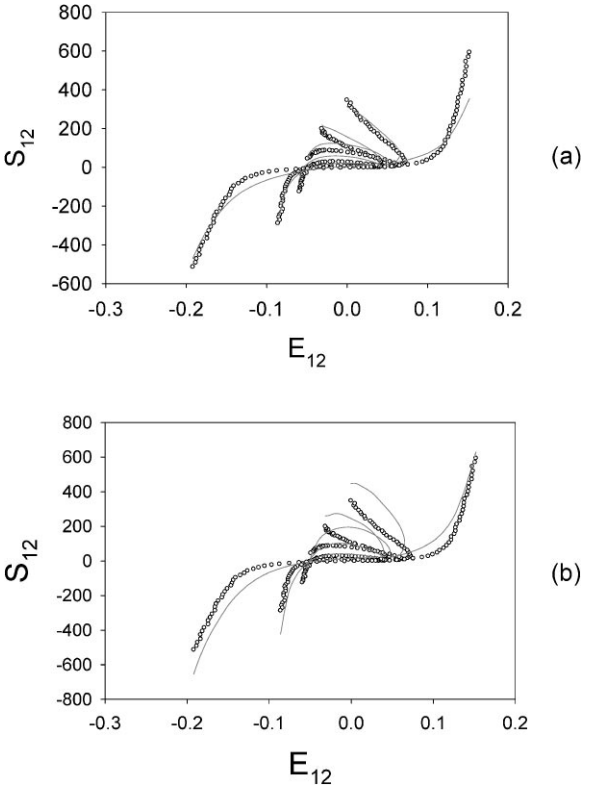

Figure 7 In-plane shear fit results for the eight-parameter model fit to (*a*) Set I only and predicting the Set II response, and (*b*) all data simultaneously. As expected, the fit to Set I demonstrated a better fit to both the inner test protocols (Set I), but also demonstrated reasonable predictive capabilities.

characterization and offer insight into the function, structure, and mechanics of tissue components. Structural constitutive models have been developed for a variety of intact tissues and tissue components including lung (45), collagen (46, 47), cartilage (48), passive myocardium (49), heart valves (41), and maturing skin (50).

Perhaps the most complete approach for structural constitutive modeling for soft tissues has been developed by Lanir et al. (51–53). In this approach, the tissue total strain energy is assumed to be the sum of the individual fiber strain energies, linked through appropriate tensor transformation from the fiber coordinates to the global tissue coordinates. However, critical structural information (such as fiber orientations) modeled using assumed statistical distributions (usually Gaussian), with the distribution parameters numerically estimated from statistical fits to the mechanical testing data.

Using bovine pericardium, Zioupos et al. (32) attempted to estimate the angular distribution of collagen fibers from uniaxial tensile experiments. However, the accuracy of this method is uncertain because the correlation between fiber orientation and ultimate tensile strength may be skewed by the large fiber rotations that exist under uniaxial loading conditions. In general, integration of quantitative morphology into structural constitutive models has yet to be achieved in the biomechanics literature. Thus, full realization of the utility of structural approaches continues to be limited without direct quantitative structural information to either validate structural model predictions or for direct implementation into the model.

In the SALS technique (36), Helium-Neon (HeNe) laser light is passed through a tissue specimen. The spatial intensity distribution of the resulting scattered light, $I(\theta)$, represents the sum of all structural information within the light beam envelope. HeNe laser light is used because its wavelength ($\lambda = 632.8$ nm) is within an order of magnitude of the diameter of the collagen and elastin fibers. Specifically, from $I(\theta)$ the angular distribution of tissue fibers can be directly obtained (54).

The availability of quantitative fiber architectural information obtainable by SALS motivated the following study (55): a structural formulation incorporating the discrete quantitative fiber architectural data derived from SALS based on Lanir (51, 56, 57). To demonstrate the approach, biaxial mechanical and fiber orientation data for native bovine pericardium was used from an earlier study (10). Two material models were utilized for the fiber stress-strain relationship, and insights into the planar mechanical properties of soft collagenous tissues were elucidated.

The distribution of collagen fiber angles was directly measured using SALS because the angular distribution of scattered light $I(\theta)$ is directly proportional to the angular distribution of fibers (36). A 2.54-mm rectilinear scanning grid was used resulting in 625 tests per specimen, with $I(\theta)$ measured using 1° increments (10). The mean scattered light intensity distribution, $\bar{I}(\theta)$, was computed for each specimen by averaging the values of $I(\theta)$ for each value of θ from all test locations.

For structural model implantation, it is necessary to determine the statistical distribution function of the angular distribution of the collagen fibers, $R(\theta)$. Specifically, $R(\theta)d\theta$ is defined as the fraction of collagen fibers oriented between θ and $\theta + d\theta$ and subjected to the normalization constraint $\int_{-\pi/2}^{\pi/2} R(\theta)d\theta = 1$. $R(\theta)$ was determined directly from the mean scattered light distribution $\bar{I}(\theta)$ for each specimen using

$$R(\theta) = \frac{\bar{I}(\theta)}{\sum_{\theta=-\pi/2}^{\theta=\pi/2} \bar{I}(\theta)\Delta\theta}, \qquad (25)$$

where, because $\bar{I}(\theta)$ is measured in discrete 1° increments (36), $\Delta\theta = \pi/180$. Because of the high structural consistency of the test specimens, local variations in $I(\theta)$ were small and $\bar{I}(\theta)$ was considered to be representative of the whole specimen (Figure 8*a*). For comparison to native heart valve fiber structure, the pericardial $R(\theta)$ demonstrated a broader distribution (41) (Figure 1*b*).

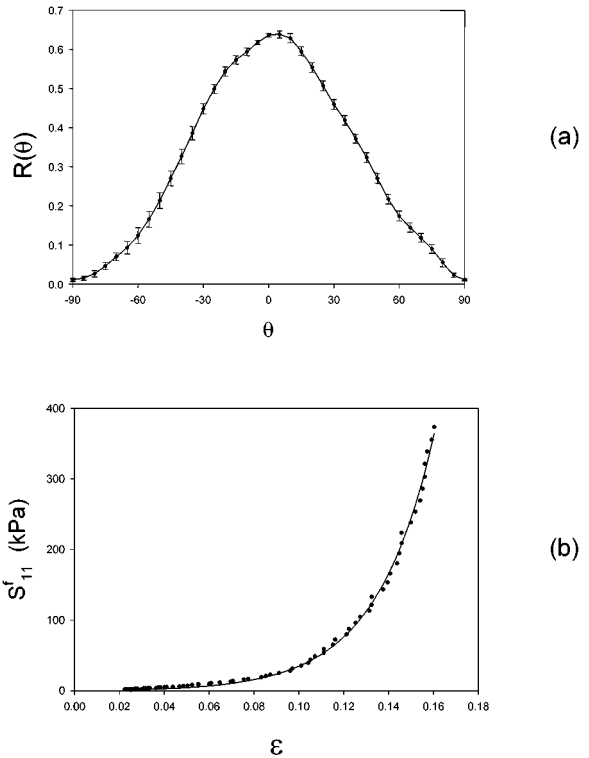

Figure 8 (*a*) The fiber angular distribution R(θ) for native bovine pericardium from one specimen demonstrating the structural regularity, as indicated by relatively small variations R(θ) (error bars = 1 standard error). (*b*) A representative example of the effective fiber stress-strain curve, along with the fit of the two-parameter fiber stress-strain law, demonstrating an excellent fit to the data.

A concern in the application of a structural constitutive model was how the externally applied biaxial strains actually translated to local fiber strains. Under the assumption of affine transformation, local fiber strains are equal to the tensorial transformation of the global tissue strains. However, the complexity of tissue structures may induce local irregularities, possibly causing nonuniform fiber strains. Information on local fiber strains under biaxial stretch for pericardium or similar tissues has not been previously reported.

Measurement of changes in collagen fiber crimp offers a means to estimate local fiber strains. In planar tissues, the collagen fibers can also undergo large rotations as well as stretch, making tracking of individual tissue areas difficult and potentially confounding measurements. However, under equibiaxial strain, the $E_{12} = 0$ and there is no fiber rotation, so that each fiber is subjected to the same uniaxial strain level equal to the equibiaxial strain level (58). Thus, changes in crimp period

will be equal for all collagen fibers in a tissue subjected to an equibiaxial strain state.

Based on these considerations, we utilized a specialized biaxial stretching device developed in our lab that allows for the biaxial stretch under real-time strain control and simultaneous SALS measurements (54). Six bovine pericardial specimens were prepared as above (including optical markers) and maintained in the optically cleared dehydrated state. Each specimen was first placed under a stereo optical microscope equipped with a charge-coupled device (CCD) camera and *trans*-illuminated with polarized light. Because the specimen was cleared, collagen crimp structure could be visualized throughout the total specimen thickness. Using a net magnification resulting in a resolution of 3.9 pixels/μm, the crimp period was measured within the region delimited by the optical markers at six evenly spaced locations. At each location, a total of six images were taken, one at the upper surface and the remaining five taken at evenly spaced increments through the thickness of the specimen by changing the focus.

Crimp periods were determined using commercial image-processing software (SigmaScan Pro, Jandel Scientific, Inc.). Crimp periods were defined as the distance between successive fiber crests, which were identified as light/dark transitions under polarized light. After the crimp measurements were taken in the undeformed state as above, the specimens were first rehydrated in room temperature normal saline for 2 h, then stretched to an equibiaxial strain (i.e., $E_{11} = E_{22}$) of 0.16, then glutaraldehyde treated in the stretched state overnight to fix the tissue structure at the stretched state. The specimens were then removed, recleared, and the crimp dimensions reanalyzed in the deformed state as above.

A general structural approach for constitutive modeling for planar collagenous tissues is presented, based upon the theoretical work of Lanir (51, 53). It is assumed that a representative volume element (RVE) can be identified that is large enough to represent the processes associated with the microstructure of the material in some average sense, yet small compared to the characteristic length scale of the microstructure, i.e., the tissue thickness. The RVE is treated as a 3-D continuum, and it is assumed that the material can be modeled as a hyperelastic solid, so that

$$\mathbf{S} = \frac{\partial W}{\partial \mathbf{E}}, \tag{26}$$

where **S** and **E** are the second Piola-Kirchoff stress and Green-Lagrange strain tensors, respectively, and W is the tissue strain energy density per unit volume.

Within the RVE, the following assumptions are made:

1. The pericardium can be idealized as a planar network of collagen fibers embedded in a compliant ground substance (i.e., the matrix). Because pericardium contains only a small amount of elastin (59), its contribution was ignored. Further, the hydrostatic forces generated by the matrix are considered negligible compared to the fiber forces and were also ignored.
2. The collagen fibers are undulated, which gradually disappears with stretch. The load required to straighten the collagen fiber is considered negligible

compared to the load transmitted by the stretched fibers. Hence, collagen fibers transmit load only if stretched beyond the point where all the undulations have disappeared and are assumed to be linearly elastic.

3. The degree of fiber undulation can vary considerably. At the tissue level, the gradual straightening of the linear elastic collagen fibers with variable undulations produces the classic nonlinear stress-strain relationship (8).
4. The fiber strain can be computed from the tensorial transformation of the global strain tensor referenced to fiber coordinates (i.e., the affine transformation assumptions).
5. The strain energy function of the tissue is the sum of the individual fiber strain energies.

Assumption 4 implies that the uniaxial strain ε along each fiber can be determined from the global tissue strain state $\mathbf{E}$ using

$$\varepsilon = \mathbf{N}^{\mathrm{T}}\,\mathbf{E}\mathbf{N}, \tag{27}$$

where $\mathbf{N} = \cos\theta\ \hat{\mathrm{i}} + \sin\theta\ \hat{\mathrm{j}}$ is the unit vector parallel to the fiber's long axis, which makes an angle θ with respect to the x_1 axis. Following Equation 12, it is convenient to express the effective collagen fiber stress as a second Piola-Kirchhoff stress, $\mathbf{S}^{\mathrm{f}}$. Because it is assumed that each fiber can only support load along its axis, $\mathbf{S}^{\mathrm{f}}(\varepsilon) = S^{\mathrm{f}}_{11}(\varepsilon)$, with all other components equaling zero.

To simulate the effective collagen fiber stress-strain law, two models were utilized. For the first model, the simplest formulation (including the fewest number of parameters) was desired, which incorporated the effects of collagen volume fraction, uncrimping, and the intrinsic properties of collagen. For this approach, the following exponential form was used:

$$S^{\mathrm{f}}_{11}(\varepsilon) = \mathrm{A}\,[\exp(\mathrm{B}\varepsilon) - 1], \tag{28}$$

where A and B are positive constants.

In the second model, the fiber recruitment and linear elastic collagen properties of the collagen fibers (following assumptions 2 and 3) were incorporated. A stochastic approach is used to represent the distribution of fiber slack length as a function of fiber strain. Here, ε_{a} and ε_{s} are the actual and straightened fiber strains, respectively, and are related using $\varepsilon_{\mathrm{a}} = \frac{\varepsilon-\varepsilon_{\mathrm{s}}}{1+2\varepsilon_{\mathrm{s}}}$, where ε is the total fiber strain given by Equation 27. The gradual recruitment of fibers with fiber strain ε (assumption 3) is simulated by a statistical distribution of $\mathrm{D}(\varepsilon)$. Assuming each fiber has an elastic modulus K, the fiber stress-strain relationship is thus (51)

$$S^{\mathrm{f}}_{11} = \mathrm{K}\int_0^{\varepsilon} \mathrm{D}(\mathrm{x})\frac{\varepsilon - \mathrm{x}}{1+2\mathrm{x}}\mathrm{dx}. \tag{29}$$

Note that for convenience, K incorporates the collagen fiber volume fraction.

For the present study, $D(\varepsilon_s)$ was approximated with a Gamma distribution:

$$D(\varepsilon_s) = \frac{1}{\beta^\alpha \Gamma(\alpha)} \varepsilon_s^{\alpha-1} \exp\left(\frac{-\varepsilon_s}{\beta}\right), \tag{30}$$

which has a mean $\alpha\beta$ and variance $\alpha\beta^2$, where α and β are positive constants. Gamma distributions are attractive in that the lower bound is zero, preventing unrealistic "negative" crimp values. Physically, $D(\varepsilon_s)$ represents the fraction of fiber fully straightened between ε and $\varepsilon + \Delta\varepsilon$ For this second model, there are a total of three material parameters: K, α, and β.

Based on the assumption 5, the total tissue strain energy W can be expressed as

$$W = \int_{-\pi/2}^{\pi/2} R(\theta) w(\varepsilon)\, d\theta, \tag{31}$$

where w is the fiber strain energy function. From Equation 2, the tissue stress-strain relationship is given by (56)

$$\mathbf{S} = \int_{-\pi/2}^{\pi/2} R(\theta) S_{11}^f(\varepsilon)[\mathbf{N} \otimes \mathbf{N}]\, d\theta, \tag{32}$$

where $\otimes$ indicates external multiplication so that $[\mathbf{N} \otimes \mathbf{N}]_{ij} = N_i N_j$. In component form, Equation 31 becomes

$$\begin{aligned} S_{11} &= \int_{-\pi/2}^{\pi/2} R(\theta) S_{11}^f(\varepsilon) \cos^2\theta\, d\theta \\ S_{12} &= \int_{-\pi/2}^{\pi/2} R(\theta) S_{11}^f(\varepsilon) \cos\theta \sin\theta\, d\theta \\ S_{22} &= \int_{-\pi/2}^{\pi/2} R(\theta) S_{11}^f(\varepsilon) \sin^2\theta\, d\theta. \end{aligned} \tag{33}$$

A unique feature of the current approach is that the fiber angular distribution function $R(\theta)$ was determined directly from the mean scattered light distribution $I(\theta)$ of the specimen. Equations 33 were thus solved numerically using Romberg integration (60), with $S_{11}^f(\varepsilon)$ set to zero when $\varepsilon \leq 0$ because fibers cannot support load when compressed.

An important feature of Equations 33 is that by summing the two expressions for normal stresses under equibiaxial strain conditions ($E_{11} = E_{22}$, $S_{12} = E_{12} = 0$), the fiber stress-strain law can be obtained directly from the experimental data using $S_{11}^f = S_{11} + S_{22}$ (53). Thus, the material parameters for $S_{11}^f(\varepsilon)$ were experimentally

determined directly from the equibiaxial test data, using the Marquardt-Levenberg nonlinear least-squares algorithm (60). Moreover, because R(θ) was determined experimentally, only the parameters associated with the fiber stress-strain material laws need be determined for the complete model.

Results for the crimp periods were generally consistent with previously reported values for bovine pericardium (61), with values ranging from 24 μm to 29 μm in the reference state. After the application of an equibiaxial Green-Lagrange strain level of 0.16 (equivalent to 15% strain), the mean collagen fiber crimp period increased in value ranging 27 μm to 34 μm. On a specimen-by-specimen basis, this translated to an increase in fiber crimp period of $\sim$15%, which is consistent with the externally applied strain level. This result indicated that, at least to a first approximation, the collagen fibers deformed similarly to the macro tissue strains. Under equibiaxial strain, the angular distribution of fiber orientations did not change from the reference state as measured by SALS. Thus, collagen fiber crimp does not detectably affect the fiber orientation distribution R(θ) for pericardium as measured by SALS.

STRUCTURAL MODEL RESULTS The two-parameter fiber stress-strain law (Equation 28) fit the equibiaxial derived data quite well, with $r^2 = 0.99$ or greater (Figure 8*b*). Variations in the constants A and B were also generally low, with the mean r^2 of 0.992. The recruitment fiber material law (Equation 29) also produced good results, although slightly lower r^2 values. Both the fiber recruitment distribution (Equation 29) and the resulting stress-strain curve were very consistent, both between specimens (as evidenced by the low standard errors) and between the group and specimen means. Because Equation 28 is nonlinear, mean values for A and B cannot be used to determine a mean fiber stress-strain response; only the group values can be considered representative of the average collagen fiber stress-strain response.

For the recruitment fiber material law, the mean collagen fiber modulus K was approximately 60 MPa. The predicted values for the mean uncrimping Green-Lagrange strain was 0.24, which corresponds to a physical strain of $\sim$22%. To provide a more physically intuitive presentation of the fiber recruitment model results, the predicted D(ε) and effective fiber stress-strain responses (for both the mean specimen and group results) are plotted together in Figure 9*a*. The increasing stiffness of the fiber stress-strain curve clearly correlates with the increasing number of recruited fibers. Integration of D(ε) was used to obtain the cumulative distribution function F(ε), which represents the fraction of fibers of the total that are stretched at the current strain level. For bovine pericardium, at the maximum Green-Lagrange strain level of 0.16, results for F(ε) indicate that $\sim$22% of the collagen fibers are fully straightened (Figure 9*b*).

A typical stress-strain response for native bovine pericardium for all test protocols is shown in Figure 10. Both the equi- and nonequibiaxial protocols were fit well by Equations 33 and the two-parameter fiber stress-strain law. Note that unlike our earlier studies (10), data from the nonequibiaxial protocols were not

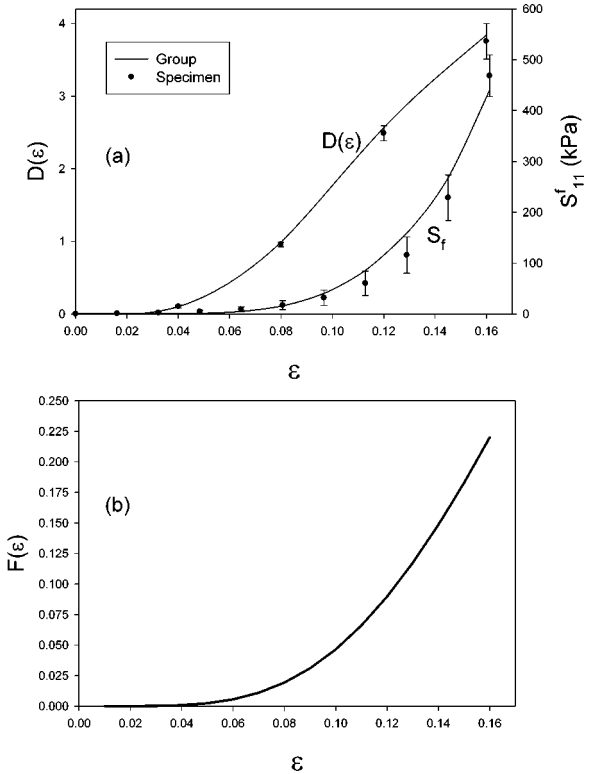

Figure 9 (*a*) The effective fiber stress-strain curve Sf using fiber recruitment model, along with the fiber recruitment function D(ε). Both mean specimen and group results are shown. Note the close correlation between the group and individual specimen means, indicating low interspecimen variations. (*b*) The "group" cumulative recruitment function F(ε), which predicted that at a Green-Lagrange strain of 0.16, ∼22% of all fibers bear load.

used to determine the material constants. Thus, the goodness of fit to the nonequibiaxial data demonstrated excellent predictive capabilities. Further, the mechanical consistency of specimens allowed us to generate meaningful results when the data from all specimens were fit simultaneously. Although having a slightly lower r^2, the grouped data coefficients fit the data reasonably well and can be considered representative of average tissue properties.

In summary, it was demonstrated that a structural constitutive modeling approach was able to accurately predict equi- and nonequibiaxial test protocols. An important aspect of this approach is that only a single equibiaxial test to determine the fiber stress-strain response and R(θ) determined by SALS are required to determine the complete planar biaxial mechanical response. Studies of collagen fiber crimp suggest that the local fiber strains follow closely the externally applied tissue

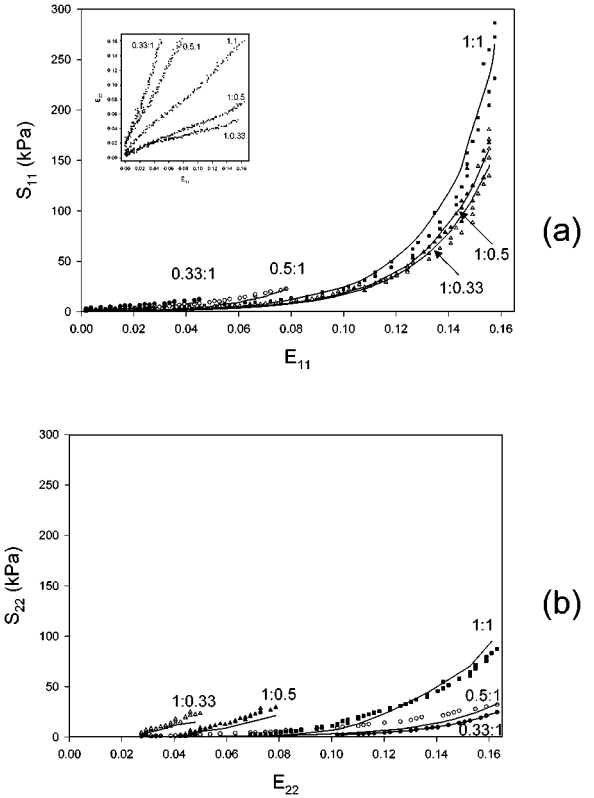

Figure 10 An example of the structural model fit to the biaxial mechanical data for native pericardium, demonstrating an excellent fit. Note that only data from the equibiaxial test was utilized to determine the form of the fiber stress-strain curve. The fit to the nonequibiaxial data demonstrates the predictive capabilities of the structural model. Labels indicate E_{11}:E_{22} ratios for each protocol. Inset: biaxial strains for each protocol with the labels indicating the E_{11}:E_{22} ratio.

strains, so that the affine transformation assumption appears to be valid. However, future evaluations will have to be performed for tissue subjected to a wider range of strain to fully validate the current approach.

7. FUTURE AREAS

From this review, one can see that our understanding of the biaxial mechanics of soft tissues is incomplete and remains a challenging scientific area. In particular, although biaxial testing techniques are sufficient for membrane tissues or tissues where thin sections can be prepared, characterization and modeling of thick-walled

organs requires true triaxial approaches. Recently, Dokos et al. developed a novel shear-test device for soft biological tissue, capable of applying simple shear deformations simultaneously in two orthogonal directions while measuring the resulting forces generated in three axes, is described (62). The device was validated using a synthetic gel, the properties of which were ascertained from independent tensile and rotational shear tests. Material parameters for the gel were fitted using neo-Hookean analytical solutions to the independent test data, and these matched the results from the device. Preliminary results obtained with rat septal myocardium are also presented to demonstrate the feasibility of the apparatus in determining the shear characteristics of living tissue.

Dokos et al. recently utilized this device to examine the shear properties of passive ventricular myocardium in six pig hearts (63). Samples ($3 \times 3 \times 3$ mm) were cut from adjacent regions of the lateral left ventricular midwall, with sides aligned with the principal material axes. Four cycles of sinusoidal simple shear (maximum shear displacements of 0.1–0.5) were applied separately to each specimen in two orthogonal directions. Resulting forces along the three axes were measured. Three specimens from each heart were tested in different orientations to cover all six modes of simple shear deformation. Passive myocardium has nonlinear viscoelastic shear properties with reproducible, directionally dependent softening as strain is increased. Shear properties were clearly anisotropic with respect to the three principal material directions: passive ventricular myocardium is least resistant to simple shear displacements imposed in the plane of the myocardial layers and most resistant to shear deformations that produce extension of the myocyte axis. Comparison of results for the six different shear modes suggests that simple shear deformation is resisted by elastic elements aligned with the microstructural axes of the tissue. The results of this study further underscore the need for actual triaxial data for the analysis of thick-walled organs.

The underlying motivations for the studies cited in this review lie not only in the understanding of natural tissue function, but also in new biomedical applications. One such application is tissue engineering, a new therapeutic approach for the functional restoration of diseased or damaged organs that utilizes cells and related biological factors to generate living tissue replacements. In mechanically demanding applications, the design and development of these tissues will invariably require a detailed understanding of the biomechanical phenomena associated with the growth, development, and engineering of soft tissue replacements. The experimental and theoretical techniques described in this review should aid in these efforts by helping to provide a rational basis for investigation and design.

ACKNOWLEDGMENTS

The authors would like to acknowledge funding by National Science Foundation Grant BES-9978858 and Edwards Lifesciences, Inc. MSS is an Established Investigator of the AHA.

The *Annual Review of Biomedical Engineering* is online at http://bioeng.annualreviews.org

LITERATURE CITED

1. Yang WH, Lu CH. 1973. General deformations of neo-hookean membranes. *J. Appl. Mech.* March:1–12
2. Wineman AS. 1976. Large axisymmetric inflation of a nonlinear viscoelastic membrane by laterial pressure. *Trans. Soc. Rheol.* 20(2):203–25
3. Choi HS, Vito RP. 1990. Two-dimensional stress-strain relationship for canine pericardium. *J. Biomech. Eng.* 112(2):153–59
4. Treloar LRG. 1975. *The Physics of Rubber Elasticity*. London: Oxford Univ. Press
5. Rivlin RS, Saunders DW. 1951. Large elastic deformations of isotropic materials, vii. Experiments on the deformation of rubber. *Philos. Trans. R. Soc.* A243:251–88
6. Spencer AJM. 1980. *Continuum Mechanics*. New York: Longman Sci. & Tech.
7. Sacks MS. 2000. Biaxial mechanical evaluation of planar biological materials. *J. Elast.* 61:99–246
8. Fung YC. 1993. *Biomechanics: Mechanical Properties of Living Tissues*. New York: Springer Verlag
9. Humphery JD. 2002. *Cardiovascular Solid Mechanics*. Berlin: Springer Verlag
10. Sacks MS, Chuong CJ. 1998. Orthotropic mechanical properties of chemically treated bovine pericardium. *Ann. Biomed. Eng.* 26(5):892–902
11. Downs J, Halperin H, Humphrey J, Yin F. 1990. An improved video-based computer tracking system for soft biomaterials testing. *IEEE Trans. Biomed. Eng.* 37:903–7
12. Humphrey J, Vawter D, Vito R. 1987. Quantification of strains in biaxially tested soft tissues. *J. Biomech.* 20(1):59–65
13. Hoffman AH, Grigg P. 1984. A method for measuring strains in soft tissue. *J. Biomech.* 10:795–800
14. Billiar KL, Sacks MS. 2000. Biaxial mechanical properties of the natural and glutaraldehyde treated aortic valve cusp–part i: experimental results. *J. Biomech. Eng.* 122(1):23–30
15. Rivlin RS, Thomas AD. 1957. Rupture of rubber: I. Characteristic energy for tearing. *J. Polym. Sci.* 10:291–318
16. Rivlin RS. 1948. Large elastic defomations of isotropic materials iv. Further developments of the general theory. *Philos. Trans. R. Soc.* A241:379–97
17. Lanir Y, Fung YC. 1974. Two-dimensional mechanical properties of rabbit skin. II. Experimental results. *J. Biomech.* 7(2):171–82
18. Lanir Y, Fung YC. 1974. Two-dimensional mechanical properties of rabbit skin. I. Experimental system. *J. Biomech.* 7(1):29–34
19. Yin FC, Tompkins WR, Peterson KL, Intaglietta M. 1972. A video-dimension analyxer. *IEEE Trans. Biomed. Eng.* 19(5): 376–81
20. Tong P, Fung YC. 1976. The stress-strain relationship for the skin. *J. Biomech.* 9(10):649–57
21. Chew PH, Yin FC, Zeger SL. 1986. Biaxial stress-strain properties of canine pericardium. *J. Mol. Cell Cardiol.* 18(6):567–78
22. Humphrey JD, Strumpf RK, Yin FCP. 1992. A constitutive theory for biomembranes: Application to epicardial mechanics. *J. Biomech. Eng.* 114:461–66
23. Humphrey JD, Vawter DL, Vito RP. 1986. Mechanical behavior of excised canine visceral pleura. *Ann. Biomed. Eng.* 14:451–66
24. Yin FCP, Chew PH, Zeger SL. 1986. An approach to quantification of biaxial tissue stress-strain data. *J. Biomech.* 19:27–37
25. Vito RP. 1980. The mechanical properties of soft tissues-i. A mechanical system for biaxial testing. *J. Biomech.* 13:947–50
26. Brossollet LJ, Vito RP. 1996. A new

approach to mechanical testing and modeling of biological tissues, with application to blood vessels. *J. Biomech. Eng.* 118:433–39

27. Humphrey JD, Strumpf RK, Yin FC. 1990. Determination of a constitutive relation for passive myocardium: I. A new functional form. *J. Biomech. Eng.* 112(3):333–39
28. Humphrey JD, Strumpf RK, Yin FC. 1990. Determination of a constitutive relation for passive myocardium: II. Parameter estimation. *J. Biomech. Eng.* 112(3):340–46
29. Sacks MS, Chuong CJ. 1993. A constitutive relation for passive right-ventricular free wall myocardium. *J. Biomech.* 26(11): 1341–45
30. May-Newman K, Yin FC. 1998. A constitutive law for mitral valve tissue. *J. Biomech. Eng.* 120(1):38–47
31. Lee JM, Courtman DW, Boughner DR. 1984. The glutaraldehyde-stablized porcine aortic valve xenograft. I. Tensile viscoelastic properties of the fresh leaflet material. *J. Biomed. Mater. Res.* 18:61–77
32. Zioupos P, Barbenel JC. 1994. Mechanics of native bovine pericardium: I. The multiangular behavior of strength and stiffness of the tissue. *Biomaterials* 15:366–73
33. Krucinski S, Vesely I, Dokainish MA, Campbell G. 1993. Numerical simulation of leaflet flexure in bioprosthetic valves mounted on rigid and expansile stents. *J. Biomech.* 26:929–43
34. Hamid MS, Sabbah HN, Stein PD. 1986. Influence of stent height upon stresses on the cusps of closed bioprosthetic valves. *J. Biomech.* 19:759–69
35. Black MM, Howard IC, Huang XC, Patterson EA. 1991. A three-dimensional analysis of a bioprosthetic heart valve. *J. Biomech.* 24:793–801
36. Sacks MS, Smith DB, Hiester ED. 1997. A small angle light scattering device for planar connective tissue microstructural analysis. *Ann. Biomed. Eng.* 25(4):678–89
37. Strumpf RK, Demer L, Yin FCP. 1983. Quantification of passive biaxial myocardial stress-strain properties. *Circulation* 68:372
38. Sacks MS, Gloeckner DC. 1999. Quantification of the fiber architecture and biaxial mechanical behavior of porcine intestinal submucosa. *J. Biomed. Mater. Res.* 46:1–10
39. May-Newman K, Yin FC. 1995. Biaxial mechanical behavior of excised porcine mitral valve leaflets. *Am. J. Physiol. Heart Circ. Physiol.* 269(4 Pt. 2):H1319–27
40. Yin FC, Strumpf RK, Chew PH, Zeger SL. 1987. Quantification of the mechanical properties of noncontracting canine myocardium under simultaneous biaxial loading. *J. Biomech.* 20(6):577–89
41. Billiar KL, Sacks MS. 2000. Biaxial mechanical properties of fresh and glutaraldehyde treated porcine aortic valve cusps: part ii—a structurally guided constitutive model. *J. Biomech. Eng.* 122(4):327–35
42. Sacks MS. 2000. A structural constitutive model for chemically treated planar connective tissues under biaxial loading. *Comput. Mech.* 26(3):243–49
43. Sacks MS. 1999. A method for planar biaxial mechanical testing that includes in-plane shear. *J. Biomech. Eng.* 121(5):551–55
44. Sun W, Sacks MS, Sellaro TL, Slaughter WS, Scott MJ. 2003. Biaxial mechanical response of bioprosthetic heart valve biomaterials to high in-plane shear. *J. Biomech. Eng.* In press
45. Mijailovich SM, Stamenovic D, Fredberg JJ. 1993. Toward a kinetic theory of connective tissue micromechanics. *J. Appl. Physiol.* 74(2):665–81
46. Comninou M, Yannas IV. 1976. Dependence of stress-strain nonlinearity of connective tissues on the geometry of collagen fibers. *J. Biomech.* 9:427–33
47. Buckley CP, Lloyd DW, Konopasek M. 1980. On the deformation of slender filaments with planar crimp: theory, numerical solution and applications to tendon collagen and textile materials. *Proc. R. Soc. London A* 372:33–64

48. Farquhar T, Dawson PR, Torzilli PA. 1990. A microstructural model for the anisotropic drained stiffness of articular cartilage. *J. Biomech. Eng.* 112(4):414–25
49. Horowitz A, Lanir Y, Yin FCP, Perl M Sheinman I, Strumpf RK. 1988. Structural three dimensional constitutive law for the passive myocardium. *J. Biomech. Eng.* 110:200–7
50. Belkoff SM, Haut RC. 1991. A structural model used to evaluate the changing microstructure of maturing rat skin. *J. Biomech.* 24(8):711–20
51. Lanir Y. 1983. Constitutive equations for fibrous connective tissues. *J. Biomech.* 16:1–12
52. Lanir Y. 1979. A structural theory for the homogeneous biaxial stress-strain relationships in flat collageneous tissues. *J. Biomech.* 12:423–36
53. Lanir Y, Lichtenstein O, Imanuel O. 1996. Optimal design of biaxial tests for structural material characterization of flat tissues. *J. Biomech. Eng.* 118:41–47
54. Billiar KL, Sacks MS. 1997. A method to quantify the fiber kinematics of planar tissues under biaxial stretch. *J. Biomech.* 30(7):753–56
55. Sacks MS. 2003. A structural constitutive model for planar collagenous tissues that integrates sals-derived fiber orientation data. *J. Biomech. Eng.* In press
56. Lanir Y. 1996. Plausibility of structural constitutive equations for swelling tissues-implications of the c-n and s-e conditions. *J. Biomech. Eng.* 118:10–16
57. Lanir Y. 1994. Plausibility of structural constitutive equations for isotropic soft tissues in finite static deformations. *J. Appl. Mech.* 61:695–702
58. Spencer A. 1972. *Deformations of Fibre-Reinforced Materials*. Glasgow: Oxford Univ. Press
59. Trowbridge E. 1989. Mechanical characteristics of pericardial tissue and their relevance to bioprosthetic design. *Crit. Rev. Biocompat.* 5:105–72
60. Press WH, Flannery BP, Teukolsky SA, Vetterling WT. 1988. *Numerical Receipes in C*. Cambridge: Cambridge Univ. Press
61. Hilbert SL, Ferrans VJ, Swanson WM. 1986. Optical methods for the nondestructive evaluation of collagen morphology in bioprosthetic heart valves. *J. Biomed. Mat. Res.* 20:1411–21
62. Dokos S, LeGrice IJ, Smaill BH, Kar J, Young AA. 2000. A triaxial-measurement shear-test device for soft biological tissues. *J. Biomech. Eng.* 122(5):471–78
63. Dokos S, Smaill BH, Young AA, LeGrice IJ. 2002. Shear properties of passive ventricular myocardium. *Am. J. Physiol. Heart Circ. Physiol.* 283(6):H2650–59

Annual Review of Biomedical Engineering
Volume 5, 2003

CONTENTS